Society For Biomaterials

Bone-forming cells with pronounced spread into the third dimension in polymer scaffolds fabricated by two-photon polymerization

J. Heitz,[1] C. Plamadeala,[1] M. Wiesbauer,[1] P. Freudenthaler,[1] R. Wollhofen,[1] J. Jacak,[1] T. A. Klar,[1] B. Magnus,[2] D. Köstner,[2] A. Weth,[3] W. Baumgartner,[3] R. Marksteiner[2]

[1]Institute of Applied Physics, Johannes Kepler University Linz, Linz, Austria
[2]Innovacell Biotechnologie AG, Innsbruck, Austria
[3]Institute of Biomedical Mechatronics, Johannes Kepler University Linz, Linz, Austria

Received 8 April 2016; revised 29 August 2016; accepted 2 November 2016
Published online 5 December 2016 in Wiley Online Library (wileyonlinelibrary.com). DOI: 10.1002/jbm.a.35959

Abstract: The main aim of this work was to stimulate bone-forming cells to produce three-dimensional networks of mineralized proteins such as those occurring in bones. This was achieved by a novel approach using a specific type of mesenchymal progenitor cells (i.e., primary fibroblast cells from human hair roots) seeded on to polymer scaffolds. We wrote polymer microstructures with one or more levels of quadratic pores on to a flexible substrate by means of two-photon polymerization using a Ti-sapphire femtosecond laser focused into a liquid acrylate-based resin containing a photoinitiator. Progenitor cells, differentiated into an osteogenic lineage by the use of medium supplemented with biochemical stimuli, can be seeded on to the hydrophilic three-dimensional scaffolds. Due to confinement to the microstructures and/or mechanical interaction with the scaffold, the cells are stimulated to produce high amounts of calcium-binding proteins, such as collagen type I, and show an increased activation of the actin cytoskeleton. The best results were obtained for quadratic pore sizes of 35 μm: the pore volumes become almost filled with both cells in close contact with the walls of the structure and with extracellular matrix material produced by the cells. © 2016 The Authors. Journal of Biomedical Materials Research Part A Published by Wiley Periodicals, Inc. J Biomed Mater Res Part A: 105A: 891–899, 2017.

Key Words: stem/progenitor cells, laser, scaffolds, tissue engineering, bone

How to cite this article: Heitz J, Plamadeala C, Wiesbauer M, Freudenthaler P, Wollhofen R, Jacak J, Klar TA, Magnus B, Köstner D, Weth A, Baumgartner W, Marksteiner R. 2017. Bone-forming cells with pronounced spread into the third dimension in polymer scaffolds fabricated by two-photon polymerization. J Biomed Mater Res Part A 2017:105A:891–899.

INTRODUCTION

For many tissue engineering applications including bone repair, it would be advantageous to replace the natural microenvironment of the cells (i.e., the extracellular matrix ECM) with three-dimensional polymer scaffolds. In recent years, numerous printing and writing techniques have evolved producing three-dimensional microstructures that mimic the ECM.[1,2] For tissue engineering, many techniques are employed in which a scaffold—usually consisting of a polymer or polymer composite material—is produced, on to which cells are seeded and adhere, and where they then proliferate. These scaffolds can be produced by a variety of techniques including direct laser-writing methods, such as stereo lithography and two-photon polymerization. Compared to stereo lithography, two-photon polymerization, which was introduced by Kawata and his group,[3] has a much better lateral resolution that can be below the diffraction limit.[4] By choice of appropriate materials, additional coating, or surface treatment, the formed structures can be made bio- and cytocompatible. For example, microstructures can be produced from the commercial photomaterial ormocer® (an organic–inorganic hybrid polymer), which enables good cell adherence and proliferation.[5] Further, cell-repellent structures produced by two-photon polymerization and combinations of cell-adherent and cell-repellent areas on the same microstructures have been described in the literature.[6] It has been recently demonstrated that microstructures with quadratic pores perform well as cell scaffolds for mural preosteogenic cells:[7] these structures consist of biodegradable poly(lactic acid) and are produced by two-photon polymerization.

In both preclinical and clinical studies, bone-marrow-derived mesenchymal stem cells (BM-MSCs) have been described as the gold standard in cell-based therapy for bone repair.[8] However, some concerns regarding the application of BM-MSCs in regenerative medicine remain, for instance, that their aspiration involves an invasive procedure and that an age-related decline occurs in their potentials for proliferation

Additional Supporting Information may be found in the online version of this article.
Correspondence to: J. Heitz; E-mail: johannes.heitz@jku.at

and osteogenic differentiation.[9] Hence, the search for new, better cells is ongoing. Reported alternative MSC-like sources include specific cells derived from adipose, skeletal, muscle, dermal, and dental tissues, as well as from fetal/neonatal tissues derived from the placenta, amniotic fluid, and umbilical cord blood.[10] We have developed a novel and unique approach to forming new bone material using primary human nonbulbar dermal sheath (NBDS) fibroblast cells taken from the sheath tissue around the hair root in human hair follicles. Although NBDS cells cannot form new hair follicles (unlike other cell types in the follicle), they possess stem–cell character.[11] Notably, it has been shown that NBDS cells produce up to five times more collagen type I than other skin-derived fibroblasts.[12] This is of particular interest in bone formation by means of tissue engineering techniques. NBDS cells express all important cell markers of mesenchymal stem cells and can therefore be expected to differentiate into other cell types within the family of mesenchymal cells of the connective tissue, which includes both fibroblasts and bone cells.[13]

As substrates for our cell scaffolds, we chose thin polymeric microscope coverslips that can be easily bent. Glycol-modified polyethylene terephthalate (PETG) is well suited as a substrate for cell scaffolds and has similar wetting and cell adhesion properties to the photoresist employed in our experiments. Polymer microstructures with several levels of quadratic pores are written on to the flexible PETG substrate by means of two-photon polymerization using a Ti-sapphire femtosecond-laser focused into a liquid acrylate-based resin containing a photoinitiator.

The main goal of this work is to fabricate polymer scaffolds, which can be filled with bone-forming cells producing three-dimensional networks of mineralized proteins such as those occurring in bones. The future application should be to repair bones in human patients by filling bone-gaps with a porous composite material consisting of acrylate-based polymer, bone-forming autologous cells, calcium-binding proteins, and calcium minerals. This composite material of customized shape shall be delivered on a suitable flexible support (for instance PETG), which finally will be removed or cut-off after implantation of the bone replacement.

MATERIALS AND METHODS

A (80/20) mixture of the two acrylate monomers pentaerythritol triacrylate (PETA, Sigma-Aldrich) and bisphenol A glycidyl methacrylate (BisGMA, Esschem Europe, Durham, UK) was used, including 2 wt % Irgacure 819 (BASF, Ludwigshafen, Germany)—an efficient photosensitive initiator of the radical polymerization chain reaction in acryl-based compounds. PETA was chosen due to its good biocompatibility,[14,15] and BisGMA (a material frequently used for dental fillings) for its mechanical stability.[16,17] The solvent propylene glycol methyl ether acetate (PGMEA) was added to achieve good mixing of the constituents and sufficient fluidity of the photoresist.

To fabricate the microstructures with quadratic pores, a two-photon polymerization setup with 15–20 mW excitation

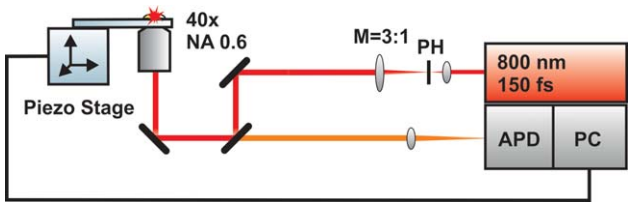

FIGURE 1. Schematics of the two-photon polarization setup. NA and M are the numerical aperture of the objective and the magnification of the telescope, respectively; PH: pin hole; APD: avalanche photodiode; PC: personal computer.

power from an 800 nm Ti-sapphire femtosecond-laser (Mai Tai, Spectra Physics, Darmstadt, Germany) was used. The laser has an 80 MHz repetition rate and produces 150 fs pulses. The setup is shown schematically in Figure 1. After mode cleaning by a 30 μm pinhole (PH) and beam expansion by means of a telescope with $M = 1{:}3$ magnification, the laser beam is focused into the liquid photoresist using a 40× objective lens (Olympus) with a numerical aperture NA = 0.6. A droplet of the liquid photoresist is placed on to the transparent substrate. An adjustable ring at the objective lens allows compensation for the refractive index mismatch between the substrate and the photoresist. The backscattered light can pass the second dichroic 90° mirror in front of the objective and is focused into the entrance of an avalanche photodiode (APD). Together with piezo actuator scanning stages (scan range 1500 × 1500 × 250 μm) and a personal computer (PC), the APD forms part of a confocal microscope used to determine the precise position of the substrate surface, which must be known because it is the starting point for structure-writing. The PC and piezo stages are also used (together with a shutter for the laser beam) to write microstructures at a typical writing velocity of 15 μm/s. Two modes of laser writing were employed: line-writing in two perpendicular lateral directions with vertical separation of 1 μm, and three-dimensional designs in stl-format constructed by a CAD program (e.g., using the free software program SketchUp Make) sliced into 1 μm thick layers by means of a g-code generator for 3D printers (e.g., using the free software program Slic3r), which were written line by line. After laser writing, the organic solvent xylole was used to wash off non-polymerized photoresist.

Tissue-culture grade PETG coverslips were chosen as substrates for our cell scaffolds. These coverslips, with a thickness of 170 μm and a diameter of 25 mm, are optically transparent, and are usually used for microscopy. They are surface-treated by the supplier (Sarstedt, Newton NC, USA) to achieve good cell adhesion and are delivered in a sterile package. For laser structure writing, the coverslips were used without modification.

Skin tissue samples for isolating of NBDS cells were obtained from volunteers in Germany with permission of the ethic committee. Hair follicles were dissected from the tissue samples and sheaths obtained for cultivation in a six-well plate. To obtain high cell quantities, the cells were further cultivated in a fibroblast-specific culture medium in an

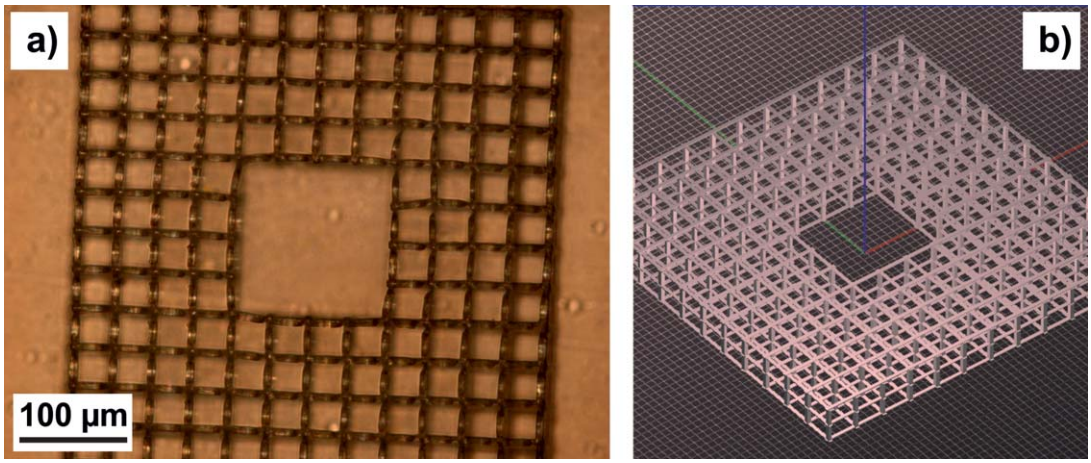

FIGURE 2. (a) Optical microscope image of a three-level PETA:BisGMA cage structure on a PETG substrate written by two-photon polymerization; (b) CAD model of the structure.

incubator. Cells were harvested by trypsinization, and the expression of mesenchymal stem cell markers was assessed by flow-cytometry with fluorescence-activated cell sorting (FACS). Finally, the cells were seeded on to the PETG coverslips with the laser-written microstructures, which were placed in a six-well cell culture microplate, and cultivated in an incubator (at 37°C and 5% CO_2). Typically, 500,000 cells were seeded per well. Prior to cell seeding, the foils were rinsed twice with a 70% ethanol solution and washed with aqua dest. A commercially available osteogenic differentiation medium (R&D Systems, Minneapolis, MN) was used to incubate the cell-seeded microstructures. Cell attachment in the structures and cell morphology were evaluated by means of phase-contrast microscopy, fluorescence microscopy, and scanning electron microscopy (SEM). For staining with Alizarin Red S (C.I.58005, Sigma Aldrich) and fluorescein isocthiocyanate (FITC) labeled phalloidin (P5262, Sigma Aldrich), the cells were fixed with formaldehyde and the samples were then analyzed using a fluorescence microscope. The same fixation method was used for immunofluorescence microscopy. As primary antibody for immunolabeling, monoclonal anticollagen type I (Clone COL-1, Sigma Aldrich) was used, and as secondary antibodies, Cy3-conjugated AffiniPure goat antimouse IgG (H + L) (115-165-166, Dianova) and Cy2-conjugated goat antirabbit (711–225-152, Dianovo) were employed. The antibodies were applied following the procedures in the product descriptions. The secondary antibodies were also used as negative controls. For SEM images, the cells were treated using standard techniques, including fixation with formaldehyde, rinsing in osmium tetroxide solution, dehydration by means of ethanol, and gold–palladium coating.

The contact angle of deionized water was measured using a device built in house. A 3 µL drop of liquid was placed on the polymer surface and viewed using a CCD camera mounted on a microscope objective with a long working distance. By drawing a rectangle, we determined the height h and the radius r of the droplet on the surface. The contact angle θ is then given approximately by $\theta = 2x$ arctan (h/r). This procedure is known as the θ /2 method.[18] The contact angle measurements were repeated 15 times. Alternatively, the water droplets and their movement were analyzed using an optical microscope (Nikon, Eclipse), which was also employed to observe the laser-written structures. SEM images of these structures were taken after gold coating.

RESULTS

Polymer microstructures on PETG substrates

Figure 2(a) shows an example microscope image of a three-level cage-like PETA:BisGMA microstructure produced by two-photon polymerization. The quadratic pores have a width of 35 µm. The distance between the levels in the 3D structures is 25 µm. Figure 2(b) illustrates the structure design, which is stored as a g-code file. Even after bending, the structure remains in close and stable contact with the PETG substrate.

For two-photon polymerization, visible or infrared light (usually from a short-pulse laser with sub-ps pulse lengths) is focused into the volume of a photosensitive material (for example, a photoresist). In the diffraction limit, the focus diameter is $d_0 = \lambda/(2\ \mathrm{NA})$ and the depth resolution $z_0 \approx \lambda\ /\ (n - (n^2 - \mathrm{NA}^2)^{0.5})$,[19] for a laser wavelength $\lambda = 800$ nm, a numerical aperture NA = 0.6, and a refraction index of the photoresist $n \approx 1.5$. Photopolymerization starts at the focus, initiated by two-photon absorption. The lateral line width of the laser-written structures is <1 µm, which is greater by a factor of about 1.5 than the diffraction limit of the focus, probably due to the relatively high laser power. In the vertical direction, the measured depth of focus is of the order of 10 µm, which corresponds to the theoretical axial resolution. Hence, while the lateral transfer of the design [Fig. 2(b)] was good, the vertical transfer was rather blurry. Figure 3 shows examples of SEM images: the structure in Figure 3(a) consists of a set of open boxes with square pores of 25 µm; Figure 3(b) shows a three-level cage structure with 35 µm square pores. The resolution in the vertical direction caused the horizontal bars in the design, which are similar to those in Figure 2(b), to be translated into sidewalls with a height of about 10 µm. 70% of the inner

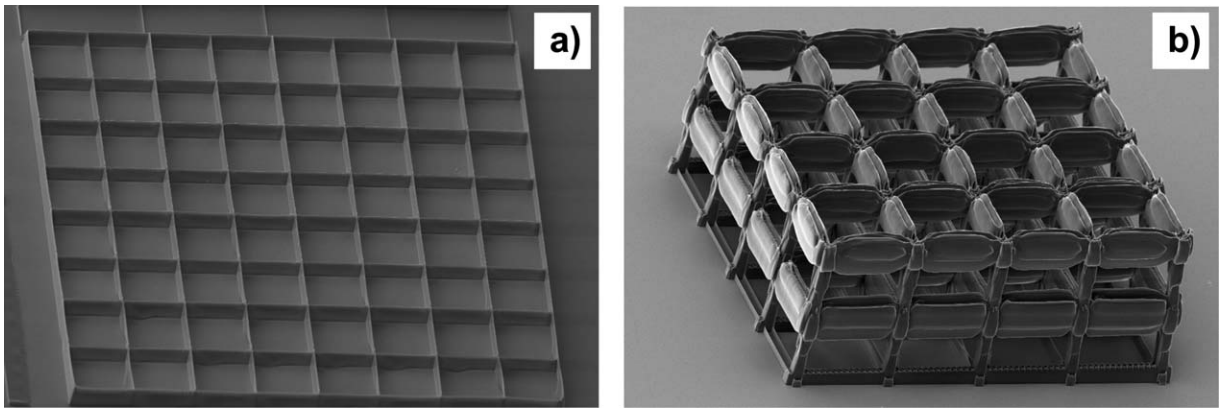

FIGURE 3. SEM images of microstructures prepared by two-photon polymerization: (a) open box structure with 25 μm square pore size, (b) three-level cage structure with 35 μm square pore size. The SEM images were taken from an angle.

volumes of the hollow sidewalls and vertical pillars were filled with a regular pattern for higher mechanical stability. The first level of the structure was only partially written due to some inaccuracy in the vertical starting position in this specific structure. Further some vertical tilt is visible. The junctions in the third levels are lower than the free-standing walls between them, which can be attributed to the structure being written from below and the laser beam passing the whole vertical pillars at junctions.

Wetting

Figure 4 shows static water contact angles of a PETG substrate (rinsed in ethanol) and a glass substrate coated with PETA:BisGMA. In the latter case, the photoresist was spin-coated on to the substrate. The sample was then dried under UV irradiation to remove the solvent and cure the photoresist. In both cases, we obtained a water contact angle θ of about 65°. The relatively small contact angle of PETG may be due to the surface treatment of the coverslips to make them cytocompatible. The PETA:BisGMA surface has a similar hydrophilic character. Figure 5 shows the microscope image of a water droplet in contact with an open box structure with 20 μm square pore size. The interface of the liquid with the structure is not smooth but follows the square pattern. The individual pores are completely filled with water, probably due to capillary forces. During drying, water is retained longer in the pores than on the flat surface.

NBDS cell differentiation

NBDS cells were trypsinized after 4 days in standard fibroblast culture medium (2.39×10^6 cells/mL). Subsequently, 25,000 cells were used for flow-cytometry immunophenotyping analysis. FACS analysis of the mesenchymal stem cell (MSC) markers[8,10] showed antigen expression of the marker CD90 (98.92%), CD73 (97.34%), and CD105 (80.33%), while the hematopoietic markers CD34 (8.3%), and CD45 (1.53%) were not expressed in significant quantities. Furthermore, NBDS cells showed high expression level for CD49b (98.18%), and CD29 (98.9%), which represent typical integrins. The results of the flow-cytometry are shown in Supporting Information 1.

Figure 6 presents microscope images of NBDS cells cultured for 7 days in standard fibroblast culture medium (SCM) and osteogenic culture medium (ODM), respectively. The NBDS cells in SCM proliferated rapidly to form a very dense cell monolayer. Also the NBDS in ODM proliferated rapidly. They were considerably smaller in cell size, but still in an overall healthy condition. They differed significantly in morphology and arrangement from the SCM-cultured NBDS cells: the cell shape is more defined and polygon-like, and the cells grew over each other in multilayers. In both images, the cells were photographed in confluence. The

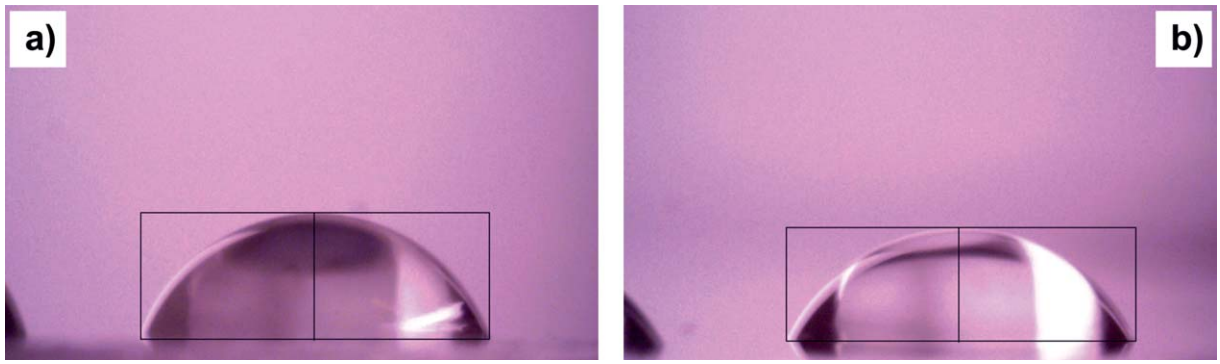

FIGURE 4. Optical microscope images of static water droplets during measurement of the water contact angle θ on (a) a PETG coverslip and (b) a glass slide coated with PETA:BisGMA. The thin black lines inserted are used for contact-angle evaluation by the $\theta/2$ method.

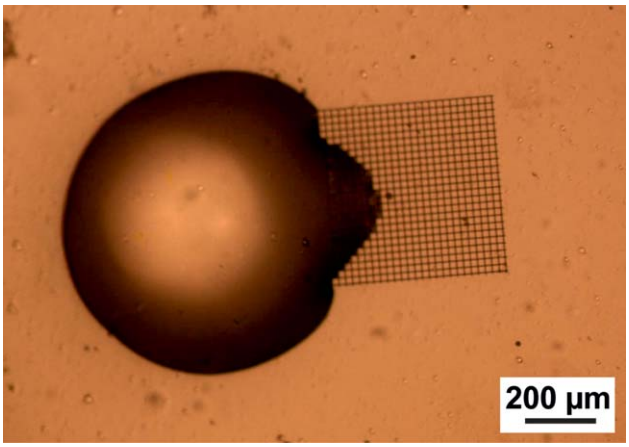

FIGURE 5. Optical microscope image of a water droplet on a PETG substrate in contact with an open box PETA:BisGMA microstructure with 20 µm square pore size written by two-photon polymerization.

formation of multilayers of ODM-cultured cells cannot only be attributed to different doubling times; for SCM-cultured cells, proliferation seems to stop when confluence is reached. This became more obvious when the experiment continued for another two weeks (data shown in Supplementary Information 2): the cells in ODM formed increasing numbers of multilayers, while the cells in SCM remained in one monolayer with nearly unchanging cell size and shape.

Differentiated NBDS in three-dimensional scaffolds

Figure 7 shows microscope images at two different magnifications of a cage microstructure with 35 µm square pores on a PETG substrate seeded with NBDS cells, and then cultivated in ODM. Many of the pores are filled with cells, and cells also grow on the flat PETG substrate. Obviously, the cell morphology in the pores differs considerably from that on the flat substrate. The cells almost fill the pores, and are small and in close contact with the pore walls. On the PETG substrate, the NBDS cells are elongated and flat, with a length greater than the pore diameter. We conducted comparative experiments with larger and smaller pore sizes. For structures with pore sizes of 25 µm, fewer pores were filled with cells than for a structure with 35 µm pores on the same substrate. On the basis of results from one-level laser-written structures similar to that in Figure 3(a), we concluded that 25 µm square pores are too small for the cells, while structures with 50 µm square pores have less influence on cell shape and spread into the third dimension than structures with 35 µm square pores. Example results are shown in Supporting Information 3. The cell-filled structures in Figure 7 bulge—an effect we observed repeatedly and which is particularly obvious at higher magnification. For structures without cells but stored in the culture medium in the incubator for the same amount of time, however, the lines remained straight.

Figure 8(a) shows SEM images of NBDS cells in a three-level cage microstructure on a flat PETG substrate. In this example, the cells were cultivated in ODM for 15 days. Again, there is a considerable difference in cell morphology between cells in the structure and those on the flat substrate. On the flat PETG substrate, the cells are flat (i.e., they exhibit two-dimensional growth), have an elongated shape, and form dense multilayers. In the scaffold structure, the cells grow in the third dimension and are in contact with the scaffold walls. Figure 8(b) shows a magnification of a part of Figure 8(a). Here, it can be seen that the pores are not only filled with cells, but that there is also fibrous extracellular material.

Figure 9(a) shows a phase-contrast microscope image of a cage microstructure with three levels and 35 µm square pores on a PETG substrate, seeded with NBDS cells, after 15 days of cultivation in ODM. Small precipitations were detected at high concentrations around the microstructure. To determine the origin of these precipitations, the sample was stained with Alizarin Red, which is a common indicator for calcium compounds.[20] Figure 9(b) shows the fluorescence microscope image of the same sample. Very strong staining was detected on and around the microstructure. Overlaying phase-contrast with fluorescence images clearly proves the link between the 3D structure and the calcium

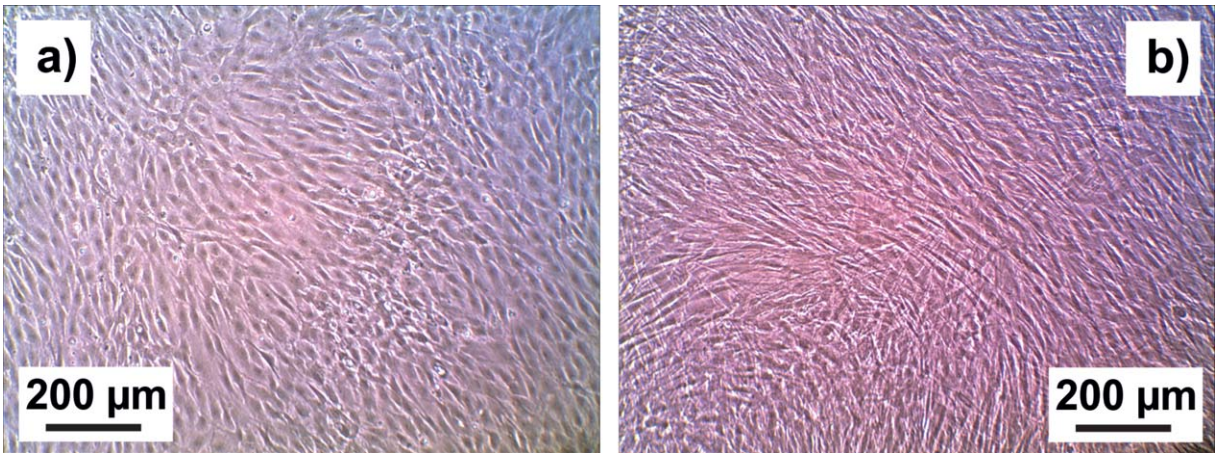

FIGURE 6. Optical microscope images of NBDS cells cultured for 7 days in (a) standard fibroblast culture medium (SCM) and (b) osteogenic culture medium (ODM). Both images have the same magnification.

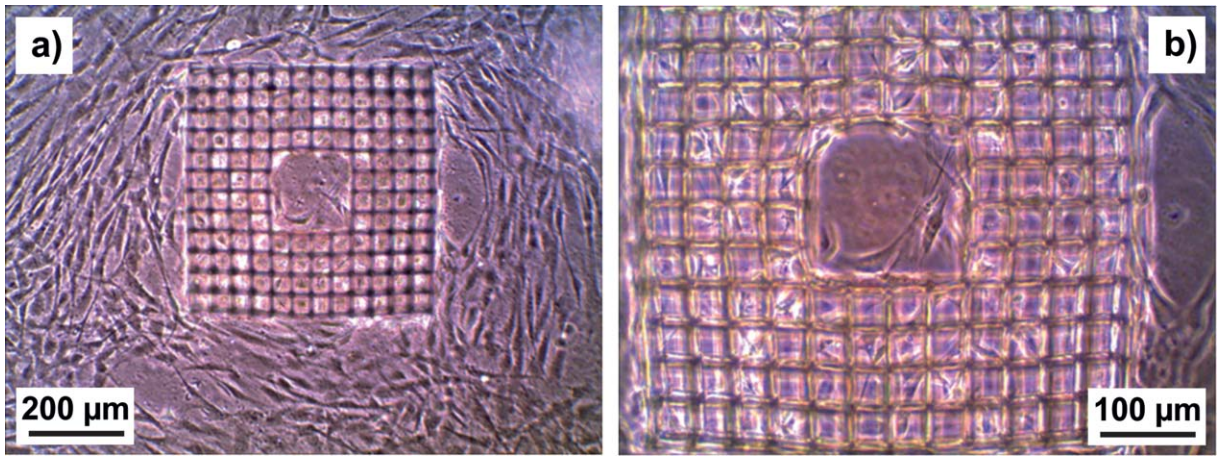

FIGURE 7. Optical microscope images at two different magnifications of a cage microstructure with 35 µm square pores on a PETG substrate seeded with NBDS cells and cultured in ODM. Both images show the same sample.

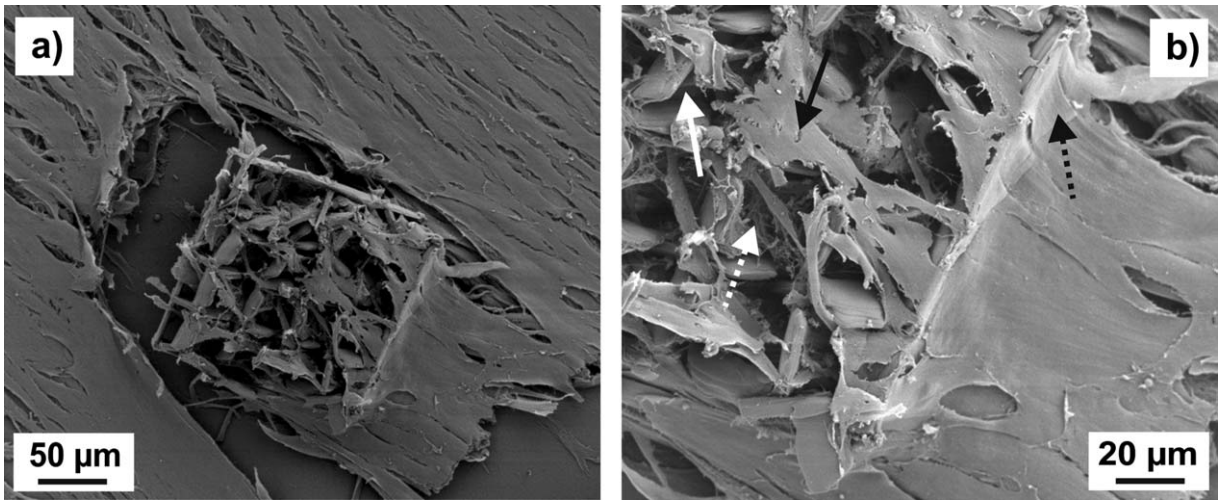

FIGURE 8. SEM images at two different magnifications of a cage microstructure with 35 µm square pores on a PETG substrate seeded with NBDS cells and cultured in ODM. Both images show the same sample. In (b), the straight white arrow points to part of a pore sidewall, the straight black arrow to a cell inside the structure, the dashed white arrow to an area which is rich in fibrous extracellular material, and the dashed black arrow to a cell part at the outer rim of the structure.

precipitations. The results on Alizarin Red staining in Figure 10 were reproduced in experiments with different cell scaffolds and independent cell batches.

Compared to NBDS cells grown on the flat PETG surface, NBDS cells in (and around) the cage microstructures show considerably increased collagen type I production and

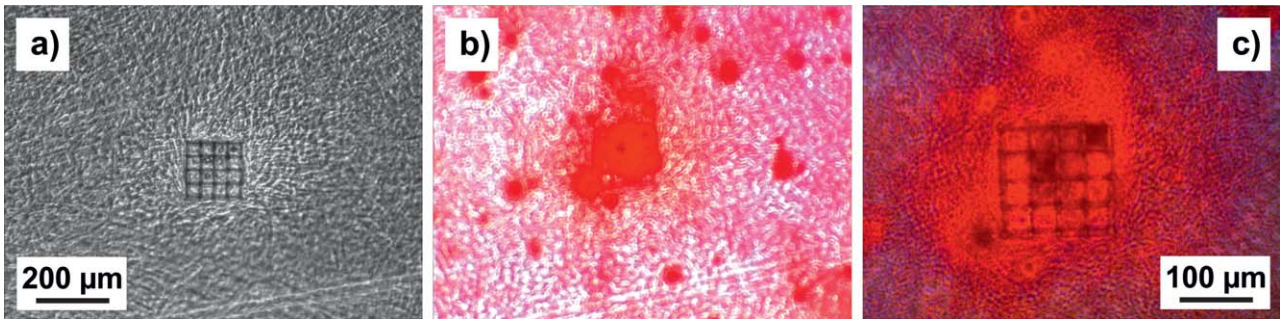

FIGURE 9. (a) Phase-contrast image of a cage microstructure with 35 µm square pores on a PETG substrate seeded with NBDS cells cultured in ODM; (b) fluorescence microscope image of the sample in (a) stained with Alizarin Red; (c) phase-contrast image in (a) overlaid with fluorescence image in (b).

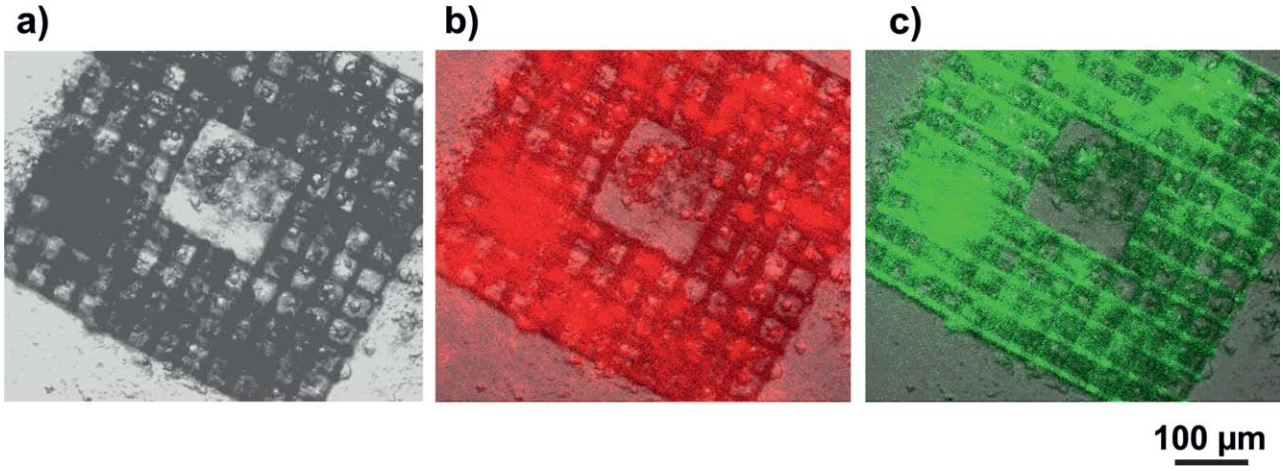

FIGURE 10. (a) Bright-field microscope image of a cage microstructure with 35 µm square pores on a PETG substrate seeded with NBDS cells cultured in ODM; (b) image (a) overlaid with an immunofluorescence image of red fluorescent collagen type I antibodies (same sample); (c) image (a) overlaid with a fluorescence image of FITC-labeled phalloidin (same sample).

increased activation of filamentous actin (F-actin) after three weeks of cultivation in ODM. This is shown in Figure 10 in the fluorescence microscope images of collagen type I antibodies and FITC-labeled phalloidin. The latter agent is known for its tight and selective binding to F-actin, a main compound of the cytoskeleton. Both fluorescence images in Figure 10 were taken from the same sample using two different fluorescence channels. As in the Alizarin Red images, we see collagen type I signals not only for cells inside but also for those around the laser-written structure.

DISCUSSION

We attribute the bulging phenomenon observed in Figure 7 to mechanical action of the cells on the walls of the scaffolds structure. The mechanical forces exerted by the NBDS fibroblast cells on the walls may be similar to those resulting in the bending of polydimethyl siloxane (PDMS) micropillar arrays described in the literature.[21] This mechanical action may also explain the observation in Figure 8, where it seems that the cells exert forces on the scaffold walls, which leads to partial destruction of the polymer structure.

The extracellular material visible in Figure 8(b) is most probably mainly collagen, which is the most abundant protein in the ECM of the human body and which is known to be produced in high amounts by NBDS cells.[12] Collagen—or, more precisely, collagen type I—is also the major constituent of natural bone. The collagen matrix in the bones is filled with mineral particles, in particular hydroxyapatite and other calcium compounds. The binding between these mineral compounds and extracellular collagen is promoted by the peptide hormone osteocalcin. Therefore, we concluded from the positive result of the Alizarin Red staining, which indicates the presence of calcium compounds, that the cells inside the scaffold were producing mineralized collagen. However, Alizarin Red staining is only an indirect proof for collagen, therefore we performed as a control experiment the test with fluorescence-labeled collagen type I antibodies shown in Figure 10(b). The increased production of collagen type I is in good agreement with the results from the Alizarin Red staining in Figure 9.

Another control experiment was the staining for F-actin shown in Figure 10(c). As F-actin is important for cell stiffness,[22] cells with high actin activation can be expected to be stiffer than those with low actin activation. This would correspond to the transition from relatively soft fibroblasts outside the scaffold to harder osteoblast-like cells inside. The latter type of cells would produce a higher amount of mineralized collagen in accordance with the results discussed in the previous paragraph.

We are the first to show by proof of principle that NBDS cells seeded on a three-dimensional scaffold and cultured in ODM can be stimulated to differentiate into osteoblast-like cells producing more mineralized ECM material than NBDS cell cultured under the same conditions on a flat substrate. This makes NBDS cells an innovative and promising alternative to conventionally used MSC sources. To our knowledge, our work is one of the few studies using primary human dermal fibroblast cells with the aim of scaffold mediated bone generation and the NDBS cells as source have the advantage that their explantations is based on the methods of hair transplantation. To mimic the human physiology of bone formation, the stimulating effect in terms of pore size, matrix stiffness, and ability to receive nutrients can only be provided by a suitable three-dimensional scaffold structure. These scaffolds were produced by laser-writing in acryl- or methacryl-based polymers. There are some concerns that their monomers or degradation products may be cytotoxic.[17,23] However, studies have shown that monomers like, for instance, PETA can be used for bone tissue engineering.[14,24] Cytotoxicity seems to be no serious problem for the polymerized material and alternative scaffold materials are under development.

Acryl- or methacryl-based polymers are already commonly employed in dentistry for tooth fillings. A promising field of application of the enhanced stimulation of cells to produce ECM due to 3D structures is also in dentistry (i.e., in dental surgery): gaps

in the jaw bone following tooth loss could be filled by reconstructing bone to provide a stable foundation for dental implants.[25] In line with the current trend toward personalized medicine, laser-writing techniques would allow individualized scaffolds to be constructed for each patient. As shown in the ring structure example (Figs. 2 and 7), the aim is not to fill the volume of the future bone-scaffold completely with cell-filled polymer structures, but to leave spaces which should allow neovascularization and metabolism. Producing a scaled-up structure of about 1 cm^3, which would be required for the jaw–bone application in humans, seems to be feasible—if demanding—using more conventional laser writing or 3D printing techniques. The two-photon polymerization technique employed in this work is better suited to create such small structures. The problem of limited spatial resolution in conventional techniques may be overcome by cyclic mechanical straining of cell scaffolds seeded with NBDS cells, which can also be expected to promote cell differentiation.[26–28] As the PETG substrates are flexible, cyclic bending of the NBDS cells in the cell scaffolds would be possible in our case, which should have an additional stimulating effect.

The mechanisms which stimulate the NBDS cells to produce mineralized collagen are not yet understood in detail. However, the cells are placed in a confined three-dimensional environment similar to that of bone-building cells under physiological conditions in the spongious bone. As in nature, they are in close contact with a cytocompatible extracellular material with which they interact via mechanical stress and strain. The stiffness of the scaffold walls and/or the collagen matrix may also play an important role for cell differentiation into the osteogenic lineage.[29,30] The close contact may be promoted by hydrophilic interaction between cell surface and scaffold walls (a similar effect was observed on polymer foils[27]) or by the increased area for unspecific focal adhesion. The chemical composition of the walls and the geometrical shape of the cell–material interface may also be important for the interaction between cells and extracellular material and for cell differentiation.[31] The three-dimensional growth is a characteristic property of osteoblasts that distinguishes them clearly from fibroblasts. This was clearly demonstrated, for instance, for cells derived from bone marrow stem cells cultured on various nanopatterned substrates.[32] Due to the limited vertical resolution of our two-photon polymerization setup, the pores also have an open box appearance in the cage-type structures with extended thin sidewalls, which have two gaps for the three-level structures. The open-box geometry forces the cells to grow into the third dimension. At least for square pore sizes of 35 μm and cytocompatible scaffolds, the cells settle easily inside the pores. There even seems to be a preference for doing so over growth on the flat scaffold.

The fact that the Alizarin Red staining in Figure 9(b) and (c) of and collagen type I signals in Figure 10(b) are visible not only inside but also around the laser-written structure may be attributed to cell migration or diffusion of ECM proteins. Alternatively, cells at the outer edges of the structure may grow to some extent into the third dimension to retain contact with the vertical wall (cf. the cells at the structural rim in Figure 8(b). This three-dimensional growth could be induced by stimuli which are similar to those for the cells inside the structure.

In Figure 10(c), there is some indication of autofluorescence of the acrylic polymers forming the cell cages, visible in the green channel of the fluorescence microscope, and most obvious at the junctions in the lower right corner of the image. The autofluorescence in Figure 10(c) may result from residual traces of the photoinitiator. However, most of the green fluorescence originates from pore areas that are filled with cells and extracellular matrix material. In the red channel, which is used to detect collagen type I, we see no pronounced auto-fluorescence of the acrylic polymer microstructures [Fig. 10(b)].

Based on our SEM results (Fig. 8) and fluorescence microscopy images (Figs. 9 and 10), we cannot exclude completely that the remarkable increase in fluorescence (of Alizarin Red, fluorescence-labeled collagen type I antibody, and phalloidin) of cells inside the cell cages over those growing on flat substrate is attributable—at least in part—to three-dimensional stacking. However, relatively stiff three-dimensionally growing osteoblasts in contact and intermingled with a calcium-mineralized collagen matrix supported with an appropriate polymer scaffold can be expected to yield very similar results to those shown in the figures for the areas inside the cell cages. In contrast, the flat cells arranged in parallel outside the microstructures resemble relatively soft fibroblasts producing less calcium-binding collagen. For the envisaged application in three-dimensional bone replacement, however, the fact that cells outside the microstructures show some properties of osteoblasts would not be of relevance.

There are some similarities in the way the pores are filled with cells and with water in the wetting test. As discussed above, the hydrophilic interaction may be an important reason why NBDS cell seeding is successful. Due to their wettability and water retention properties, these structures have potential applications beyond cell scaffolds, for instance, in lubrication, moisture harvesting, and cooling.

CONCLUSIONS

Our experiments demonstrated for the first time that fibroblast cells from human hair follicles can be stimulated to produce more calcium-binding extracellular fibrous material if the cells are seeded on to a three-dimensional cell scaffold with 35 μm square pore size rather than grown in normal 2D cell cultures. The three-dimensional cell scaffolds consisting of a hydrophilic acryl-based polymer were laser-written using two-photon polymerization. The extracellular material produced by the cells is probably mainly collagen. The ability to stimulate cells to produce three-dimensional networks of mineralized collagen, the main constituents of bones, may have promising medical applications, especially in the field of dental surgery.

ACKNOWLEDGMENTS

Support by the Austrian Research Promotion Agency FFG, within the scope of project 843665 3DCellStretch, and the European program H2020, within the scope of project 665337 LiNaBioFluid, is gratefully acknowledged.

REFERENCES

1. Schober A, Fernekorn U, Singh S, Schlingloff G, Gebinoga M, Hamp J, Williamson A. Mimicking the biological world: Methods for the 3D structuring of artificial cellular environments. Eng Life Sci 2013;13:352–367.
2. Ovsianikov A, Chichkov BN. Three-dimensional microfabrication by two-photon polymerization technique. Methods Mol Biol 2012; 868:311–325.
3. Maruo S, Nakamura O, Kawata S. Three-dimensional microfabrication with two-photon-absorbed photopolymerization. Opt Lett 1997;22:132–134.
4. Ostendorf A, Chichkov BN. Two-photon polymerization: A new approach to micromachining. Photon Spectra 2006;2006:26907.
5. Narayan RJ, Jin CM, Doraiswamy A, Mihailescu IN, Jelinek M, Ovsianikov A, Chichkov B, Chrisey DB. Laser processing of advanced bioceramics. Adv Eng Mater 2005;7:1083–1098.
6. Klein F, Richter B, Striebel T, Franz CM, von Freymann G, Wegener M, Bastmeyer M. Two-component polymer scaffolds for controlled three-dimensional cell culture. Adv Mat 2011;23:1341–1345.
7. Danilevicius P, Georgiadi L, Pateman CJ, Claeyssens F, Chatzinikolaidou M, Farsari M. The effect of porosity on cell ingrowth into accurately defined, laser-made, polylactide-based 3D scaffolds. Appl Surf Sci 2015;336:2–10.
8. Chatzinikolaidou M, Rekstyte S, Danilevicius P, Pontikoglou C, Papadaki H, Farsari M, Vamvakaki M. Adhesion and growth of human bone marrow mesenchymal stem cells on precise-geometry 3D organic–inorganic composite scaffolds for bone repair. Mater Sci Eng C 2015;48:301–309.
9. Zigdon-Giladi H, Rudich U, Michaeli Geller G, Evron A. Recent advances in bone regeneration using adult stem cells. World J Stem Cells 2015;7:630–640.
10. Grayson WL, Bunnell BA, Martin E, Frazier T, Hung BP, Gimble JM. Stromal cells and stem cells in clinical bone regeneration. Nat Rev Endocrinol 2015;11:140–150.
11. McElwee KJ, Kissling S, Wenzel E, Huth A, Hoffmann R. Cultured peribulbar dermal sheath cells can induce hair follicle development and contribute to the dermal sheath and dermal papilla. J Invest Derm 2003;121:1267–1275.
12. Oh JK, Kwon OS, Kim MH, Jo SJ, Han JH, Kim KH, Eun HC, Chung JH. Connective tissue sheath of hair follicle is a major source of dermal type I procollagen in human scalp. J Dermatol Sci 2012;68:194–197.
13. Alberts B, Johnson A, Lewis J, Raff M, Roberts K, Walter P. Molecular Biology of the Cell, 5th ed, New York: Garland Science; 2007.
14. Chen C, Garber L, Smoak M, Fargason C, Scherr T, Blackburn C, Bacchus S, Lopez MJ, Pojman JA, Del Piero F, Hayes DJ. *In vitro* and *in vivo* characterization of pentaerythritol triacrylate-*co*-trimethylolpropane nanocomposite scaffolds as potential bone augments and grafts. Tissue Eng A 2015;21:320–331.
15. Smoak M, Chen C, Qureshi A, Garber L, Pojman JA, Janes ME, Hayes DJ. Antimicrobial cytocompatible pentaerythritol triacrylate-*co*-trimethylolpropane composite scaffolds for orthopaedic implants. J Appl Poly Sci 2015;131:41099.
16. Liu Y, Jiang G, He G. Enhancement of entangled porous titanium by BisGMA for load-bearing biomedical applications. Mater Sci Eng C 2016;61:37–41.
17. Manojlovic D, Dramicanin MD, Milosevic M, Zekovic I, Cvijovic-Alagic I, Mitrovic N, Miletic V. Effects of a low-shrinkage methacrylate monomer and monoacylphosphine oxide photoinitiator on curing efficiency and mechanical properties of experimental resin-based composites. Mater Sci Eng C 2016;58:487–494.
18. Yuan Y, Lee TR. Contact angle and wetting properties. In: Bracco G, Holst B, editors. Surface Science Techniques. Heidelberg: Springer; 2013. p 336.
19. Fischer J, Wegener M. Three-dimensional optical laser lithography beyond the diffraction limit. Laser Photon Rev 2013;7:22–44.
20. Puchtler H, Meloan SN, Terry MS. On the history and mechanism of Alizarin Red S stains for calcium. J Histochem Cytochem 1969; 17:110–124.
21. van Hoorn H, Harkes R, Spiesz EM, Storm C, van Noort D, Ladoux B, Schmidt T. The nanoscale architecture of force-bearing focal adhesions. Nano Lett 2014;14:4257–4262.
22. Kasas S, Wang X, Hirling H, Marsault R, Huni B, Yersin A, Regazzi R, Grenningloh G, Riederer B, Forro L, Dietler G, Catsicas S. Superficial and deep changes of cellular mechanical properties following cytoskeleton disassembly. Cell Motil Cytoskelet 2005;62: 124–132.
23. Husar B, Heller C, Schwentenwein M, Mautner A, Varga F, Koch T, Stampfl J, Liska R. Biomaterials based on low cytotoxic vinyl esters for bone replacement application. Polym Chem 2011;49:4927–4934.
24. Garber L, Chen C, Kilchrist KV, Bounds C, Pojman JA, Hayes D. Thiol-acrylate nanocomposite foams for critical size bone defect repair: A novel biomaterial. J Biomed Mater Res A 2013;101:3531–3541.
25. Brown A, Zaky S, Ray H, Sfeir C. Porous magnesium/PLGA composite scaffolds for enhanced bone regeneration following tooth extraction. Acta Biomater 2015;11:543–553.
26. Chiquet M, Gelman L, Lutz R, Maier S. From mechanotransduction to extracellular matrix gene expression in fibroblasts. Biochim Biophys Acta 2009;1793:911–920.
27. Barb RA, Magnus B, Innerbichler S, Greunz T, Wiesbauer M, Marksteiner R, Stifter D, Heitz J. VUV treatment combined with mechanical strain of stretchable polymer foils resulting in cell alignment. Appl Surf Sci 2015;325:105–111.
28. Gerstmair A, Fois G, Innerbichler S, Dietl P, Felder E. A device for simultaneous live cell imaging during uni-axial mechanical strain or compression. J Appl Physiol 2009;107:613–620.
29. Engler AJ, Sen S, Sweeney H, Discher DE. Matrix elasticity directs stem cell lineage specification. Cell 2006;126:677–689.
30. Rich H, Odlyha M, Cheema U, Mudera V, Bozec L. Effects of photochemical riboflavin-mediated crosslinks on the physical properties of collagen constructs and fibrils. J Mater Sci Mater Med 2014;25:11–21.
31. Yakunin S, Fahrner M, Reisinger B, Itani H, Romanin C, Heitz J. Laser microstructuring of photomodified fluorinated ethylene propylene surface for confined growth of Chinese hamster ovary cells and single cell isolation. J Biomed Mater Res B 2012;100B: 170–176.
32. Dalby MJ, Gadegaard N, Tare R, Andar A, Riehle MO, Herzyk P, Wilkinson CDW, Oreffo ROC. The control of human mesenchymal cell differentiation using nanoscale symmetry and disorder. Nat Mater 2007;6:997–1003.